Magnetic order of the Cu planes and chains in RBa$_2$Cu$_3$O$_{6+x}$

W-H. Li and J. W. Lynn
Center for Superconductivity Research, Department of Physics, University of Maryland, College Park, Maryland 20742 and National Institute of Standards and Technology, Gaithersburg, Maryland 20899

Z. Fisk
MS-K764, Los Alamos National Laboratory, Los Alamos, New Mexico 87545

(Received 14 August 1989)

Polarized and unpolarized neutron-diffraction measurements have been taken to determine the magnetic structure of the Cu spins in the RBa$_2$Cu$_3$O$_{6+x}$ system as a function of temperature. Most of the results have been obtained on two (semiconducting) oxygen-deficient single crystals of composition NdBa$_2$Cu$_3$O$_{6.1}$ and NdBa$_2$Cu$_3$O$_{6.35}$. On cooling from the paramagnetic state, the Cu-O "plane" layers first order at a Néel temperature T_{N1} in a simple antiferromagnetic arrangement of spins, with $T_{N1}=430$ K for $x=0.1$ and $T_{N1}=230$ K for $x=0.35$, and with a saturated moment of $\sim 0.65\mu_B$. At a lower temperature T_{N2} the Cu "chain" layer also orders, with $T_{N2}=80$ and 10 K for $x=0.1$ and 0.35, respectively. Hence both transition temperatures decrease with increasing oxygen concentration in this range of x, and the qualitative behavior for these two samples is found to be identical. We have not, however, observed this low-T structure in polycrystalline samples of either YBa$_2$Cu$_3$O$_{6+x}$ or NdBa$_2$Cu$_3$O$_{6+x}$, and some possible explanations for this difference in behavior are discussed. For the single crystals in the low-T phase the Cu spins in all three copper-oxygen layers are ordered in a simple antiferromagnetic arrangement, with the magnetic unit cell double the chemical unit cell along all three crystallographic directions. On the basis of the measured integrated intensities of over 40 magnetic reflections in both ordered phases, the results can be accounted for quantitatively with the assumption of a 3d magnetic form factor on the Cu ions, with no need for a significant moment on any of the oxygen ions. At low T, site-averaged moments of $\sim 0.35\mu_B$ and $\sim 0.8\mu_B$ are obtained in the "chain" and the "plane" layers, respectively. The fact that the ordered moment on the plane layers increases in the low-T phase is direct evidence that two-dimensional quantum fluctuations play an important role in the plane layers in the high-T ordered phase. The evolution of the low-T spin structure into the high-T structure involves a noncollinear configuration in which the spins rotate as a function of temperature in the "plane" layers, while the "chain" layer becomes thermally disordered. The temperature dependence of the structure indicates that competing interactions between the layers are important, and this is discussed in detail. Finally, exploratory measurements as a function of applied magnetic field indicate that the magnetic anisotropy in the tetragonal plane is much smaller than the exchange energies.

I. INTRODUCTION

The magnetic properties of the high-T_c superconducting oxides have attracted considerable interest in an effort to understand the origin of their electronic and magnetic behavior. The initial evidence for magnetic order in these systems was obtained in La$_2$CuO$_4$ by both muon precession[1,2] and neutron scattering measurements,[3-10] and then in $\mathcal{R}$Ba$_2$Cu$_3$O$_{6+x}$ ($\mathcal{R}$ represents rare-earth element) by a number of groups including Tranquada *et al.*,[11-13] Kadowaki *et al.*,[14] Burlet *et al.*,[15] and independently by us.[16-19] Two types of antiferromagnetic transitions, involving both the "plane" layers and the "chain" layers, have been observed. In this paper we present a detailed study of the magnetic structures in both ordered phases, and describe how one structure evolves into the other.

The $\mathcal{R}$Ba$_2$Cu$_3$O$_{6+x}$ compounds[20] have a layered perovskitelike structure in which there are three copper-oxygen layers of ions stacked along the (unique) tetragonal c axis is shown in Fig. 1. Two of these layers have oxygen ions between the copper ions in both the a and b crystallographic directions. These are the so-called plane layers, and the oxygen in these layers cannot be removed. The third layer has oxygen ions only along the b axis, and is thus called the chain layer. The oxygen concentration can be readily varied in this layer from full occupancy ($x=1$) to complete depletion ($x=0$). Both the magnetic and superconducting properties are very sensitive to the oxygen concentration x in the chain layers, and a schematic phase diagram[12-24] for this class of materials is shown in Fig. 2. In the small x regime we have a tetragonal antiferromagnetic insulator, while at large x we have an orthorhombic superconductor with $a \approx b$ and $c \approx 3a$. On the other hand, the substitution of the trivalent rare-earth elements on the Y site has little effect on the superconducting properties of $\mathcal{R}$Ba$_2$Cu$_3$O$_{6+x}$, indicating that the rare-earth sublattice is electronically isolated from the superconducting electrons.

The magnetic properties in the small x regime, where the materials are tetragonal and semiconducting, have

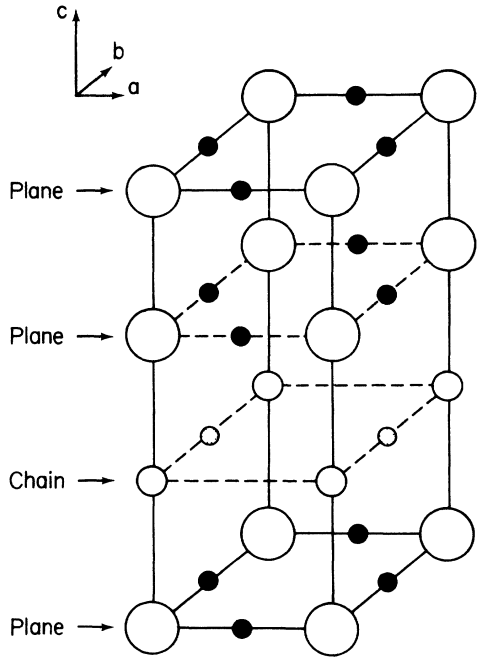

FIG. 1. The crystal structure of $\mathcal{R}Ba_2Cu_3O_7$, with only the Cu (open circles) and O ions (solid and shaded circles) in the copper-oxygen layers indicated for clarity. The rare-earth ion is located between the two plane layers, while the plane and the chain layers are separated by a BaO layer. The occupancy of the oxygen sites in the chain layer (shaded circles) can be readily varied from full occupancy ($x=1$) to full depletion ($x=0$).

proved to be very interesting. The Cu plane layers order antiferromagnetically with a Néel temperature T_N as high as 500 K as indicated in Fig. 2. This is quite a high magnetic transition temperature for a nonmetallic system. The exchange interactions are also very anisotropic,

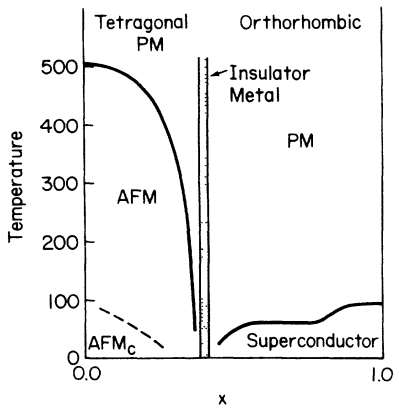

FIG. 2. Schematic phase diagram for $\mathcal{R}Ba_2Cu_3O_{6+x}$ as a function of oxygen concentration x on the chain sites. There are two antiferromagnetic phases in the small x regime: AFM, in which only the Cu spins in the plane layers are ordered, and AFM_C, in which the Cu spins in the chain layers are also ordered. At large x or at very high temperatures the Cu ions are paramagnetic (PM).

with the in-plane interactions greatly exceeding the energy represented by kT_N, while the interplanar interactions are weak.[6,25,26] Thus there are substantial two-dimensional (2D) correlations which persist well above T_N. The value of the ordered magnetic moment has also been found to decrease with increasing x, scaling approximately as T_N,[12,15] but the paramagnetic moment does not change substantially, and in fact paramagnetic moments exist within the superconducting phase.[27–29] The persistence of magnetic correlations in the superconducting phase, and the fact that the superconducting transition affects the temperature dependence of these fluctuations, have supported theories[20,30] based on magnetic pairing of the superconducting electrons. However, even if magnetism is not the origin of the pairing, it is clear that any comprehensive theory of this class of materials must include an understanding of the spin degrees of freedom.

At lower temperatures the spins on the Cu chain sites have also been observed to order antiferromagnetically.[14,16–19] The spin configuration within the chain layers is a simple antiparallel arrangement of nearest neighbors just as it is for the plane layers, while the configuration along the c axis turns out to be a simple $+-+-+-$ sequence at low temperatures. This additional ordering causes an interplanar competition between the plane and the chain layers, and results in a rich behavior of the magnetic structure as a function of temperature. The magnetic structures in the high-T and low-T phases have been briefly discussed previously.[16–19] In this paper we present a complete study of the temperature dependence of the magnetic ordering of Cu spins in $NdBa_2Cu_3O_{6+x}$, and discuss in detail how the magnetic structure evolves from its low-temperature to its high-temperature ordered phase. Our spin structure of the Cu ions is refined based on more than 40 independent single-crystal reflections obtained at several temperatures.

II. EXPERIMENTAL DETAILS

All of the neutron scattering experiments were carried out at the National Institute of Standards and Technology (formerly the National Bureau of Standards) Research Reactor. Unpolarized diffraction data were collected using a pyrolytic graphite PG(002) monochromator and PG filter, with an incident energy of either 14.8 or 28.3 meV, at the BT-9 triple-axis spectrometer. A four-circle goniometer was employed to orient the crystal. Angular collimations before and after the monochromator and analyzer (when used) were 40′ (full width at half maximum, FWHM) in all cases. Polarized-neutron measurements were performed at the BT-2 triple-axis polarized-beam spectrometer, with an incident energy of 13.5 meV. The incident beam was monochromated and polarized by a vertically magnetized focusing Heusler (111) alloy, and the polarization of the scattered neutrons was analyzed by a supermirror. A PG filter was employed to suppress higher-order wavelengths, and vertical guide fields were employed along the neutron path to prevent depolarization of the beam. Angular collimations were 60′ before the monochromator and 40′ elsewhere. All of the samples investigated were sealed in aluminum containers

filled with helium exchange gas to facilitate thermal conduction at low temperatures. A standard gas-flow cryostat or Displex refrigerator was used for the low-temperature measurements, while a vacuum furnace was employed for the measurements above room temperature. Finally, low-temperature field-dependent measurements were taken in a split-coil superconducting magnet, with a vertical field capability of 7 T.

Measurements were made on four different samples with different oxygen concentrations. Two samples were polycrystalline, with compositions $YBa_2Cu_3O_{6.13}$ and $NdBa_2Cu_3O_{6.03}$, and weighing ~ 9 g each. The other two samples were single crystals, one with composition $NdBa_2Cu_3O_{6.35}$ and weighing 9.5 mg, and a second one with composition $NdBa_2Cu_3O_{6.1}$ and weighing 45 mg. The powder samples were prepared by the usual solid-state reaction technique as described elsewhere.[31] The single-crystal samples were grown by slowly cooling from 1220 °C a Ba-rich flux of the oxides, with a small amount of PbO added to the melt.

The oxygen concentrations for the powder samples were determined by thermogravimetric analysis, and that for the two single crystals were determined by Rutherford backscattering (RBS) techniques. These results for the oxygen concentration agree quite well with the values expected based on their measured Néel temperatures T_N,[22,32] in fact the measured Néel temperatures provide the best determination of the oxide concentration. The RBS measurements as well as scanning electron microscope (SEM) measurements on the single crystals revealed a ratio of Nd:Ba:Cu of 1:2:3 within experimental error, indicating that there is no significant substitution of the rare earth onto the Ba site for these single-crystal samples. We have no indication of any Pb incorporated into the 1:2:3 matrix, but the RBS and SEM measurements cannot rule out the possibility that a small amount of Pb has substituted for the large cations in this system.

To analyze the observed magnetic intensities we must compare them with model calculations. The integrated intensity for a magnetic Bragg reflection can be written as[33]

$$I_M = CL\Omega \ , \tag{1}$$

where C is an instrumental constant that can be readily determined by the measured nuclear Bragg intensities, and L is an angular factor that depends on the type of scan performed to obtain the integrated intensity of the reflection. Ω contains the magnetic structure factor and the orientation factor, and is given by

$$\Omega = \sum_{\alpha,\beta} \langle (\delta_{\alpha\beta} - \hat{\mathbf{K}}_\alpha \cdot \hat{\mathbf{K}}_\beta) F_M(\mathbf{K},\alpha) F_M^*(\mathbf{K},\beta) \rangle_D \ , \tag{2}$$

where α and β stand for x,y,z, and $\delta_{\alpha\beta}$ is the Kronecker delta function. $\mathbf{K}$ is the scattering vector, $\hat{\mathbf{K}}_\alpha$ is the component of the unit vector of $\mathbf{K}$ along α, and the $\langle\ \rangle_D$ is an average over all possible domains. The magnetic structure factor is a vector quantity, and its component along α is given by

$$F_M(\mathbf{K},\alpha) = \sum_j \langle \mu_j^\alpha \rangle f_j(\mathbf{K}) e^{i\mathbf{K}\cdot\mathbf{r}_j} e^{-W_j} \ , \tag{3}$$

where $\langle \mu_j^\alpha \rangle$ is the thermal average of the α component of the moment on the magnetic ion located at the jth site at the position vector $\mathbf{r}_j$, W_j is the Debye-Waller factor for the jth atom, and the sum extends over all magnetic atoms in the unit cell. $f(\mathbf{K})$ is the magnetic form factor, which is the Fourier transform of the atomic magnetization density. A detailed comparison of a model calculation for the integrated intensities of the magnetic Bragg reflections can then quantitatively test the model used. We remark that Eq. (2) can often be written in a simplified form if the magnetic structure is collinear, but this is not always the case for the materials presently under investigation.

Polarized neutrons have also been used to verify that the observed temperature-dependent Bragg reflections are magnetic in origin. The technique to isolate the magnetic response using polarized neutrons has been described in detail in the literature.[34] The basic principle employed is that when a magnetic field $\mathbf{B}$ within the sample is parallel to the scattering vector $\mathbf{Q}$, all of the magnetic scattering is associated with a reversal of the neutron spin (spin-flip scattering), while for $\mathbf{B}\perp\mathbf{Q}$, the spin-flip and non-spin-flip scattering are equally probable. The nuclear scattering, on the other hand, is independent of the orientation of $\mathbf{B}$ and $\mathbf{Q}$. The spectrometer was set up so that polarized neutrons were incident upon the sample. A supermirror was then used to reflect only those neutrons that underwent a spin reversal in the sample, with the applied magnetic field first parallel and then perpendicular to the scattering vector. A subtraction of the observed intensities between the $\mathbf{B}\|\mathbf{Q}$ and $\mathbf{B}\perp\mathbf{Q}$ configurations leaves only the magnetic component, with the background and nuclear-spin incoherent scattering contributions canceling.

III. RESULTS

Before proceeding to the details of the scattering experiments and the magnetic structures, we give an overview of the magnetic behavior observed. The spins in all three layers turn out to be coupled antiferromagnetically within the tetragonal layers in both the low-T and high-T phases. Hence the magnetic unit cell is double the chemical unit cell along both directions in the tetragonal plane, requiring that the first two Miller indices h and k for the magnetic reflections be half integral if the usual convention of indexing the magnetic reflections on the basis of the chemical unit cell is used. For the unit cell along the c direction, there are two types of ordering which have been observed. At low temperatures both the chain layers and the plane layers are ordered with an antiferromagnetic sequence along the c axis like $(+-+\ -+-\ \cdots)$. This yields a magnetic unit cell double the chemical one along the c-axis direction as well, and thus the third Miller index l will also be half integral. We will refer to these peaks as "half-integral peaks."

The strongest magnetic Bragg reflection in the low-T phase turns out to be the $(\frac{1}{2}\ \frac{1}{2}\ \frac{3}{2})$ reflection, shown in Fig. 3(a), which was obtained from the $x=0.1$ crystal at $T=10$ K. The results of the polarized beam measurements made on this particular peak are shown in Fig.

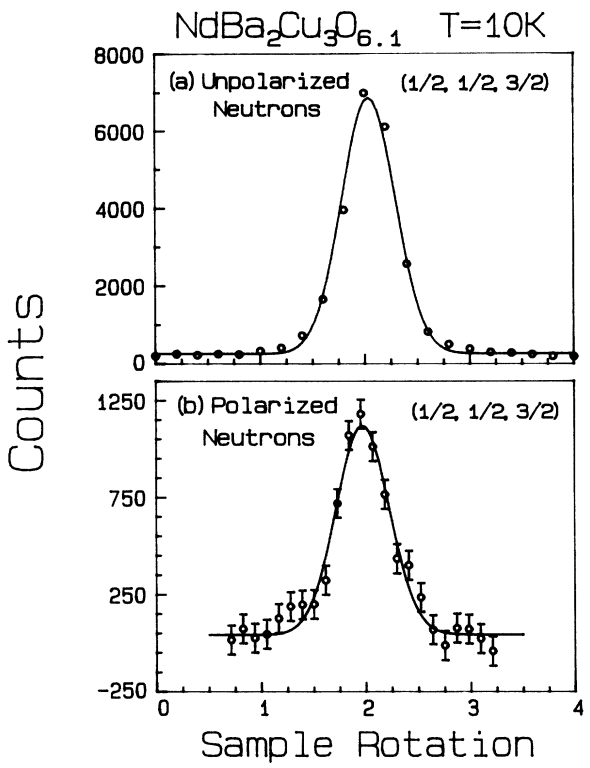

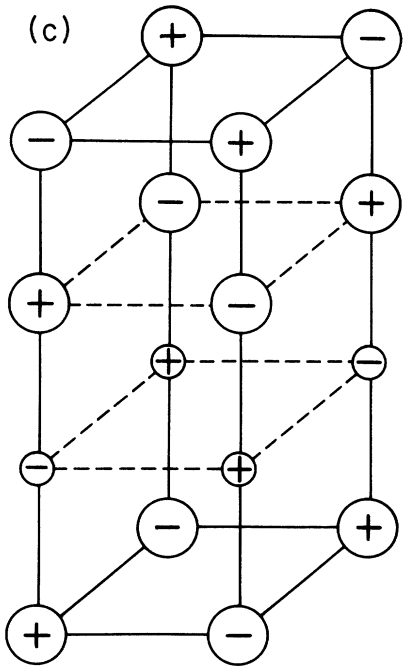

FIG. 3. The $(\frac{1}{2}\ \frac{1}{2}\ \frac{3}{2})$ Bragg reflection from the $x=0.1$ crystal at $T=10$ K is shown. (a) The unpolarized beam result. (b) The polarized beam result, where the difference of the observed intensities between the $\mathbf{B}\|\mathbf{Q}$ and $\mathbf{B}\perp\mathbf{Q}$ configurations is plotted. The data demonstrate that the scattering is magnetic in origin. The solid curves are a least-squares fit to a Gaussian (resolution) function. (c) The basic spin structure for the Cu moments at low T. There is a substantial moment on the Cu ions in the oxygen deficient chain layer (small circles).

3(b). Even though the Cu moments are quite small, the crystal is sufficiently large to obtain an excellent signal-to-noise ratio. The spin-flip scattering intensity with $\mathbf{B}\perp\mathbf{Q}$ configuration was half that with $\mathbf{B}\|\mathbf{Q}$ configuration, and the polarized-beam measurements clearly establish that the half-integral peaks are indeed wholly magnetic in origin. In addition, the relative intensities between spin-flip magnetic $(\frac{1}{2}\ \frac{1}{2}\ \frac{3}{2})$ and non-spin-flip nuclear (001) reflections are consistent with the data obtained using unpolarized neutrons. A subtraction between the data obtained with the $\mathbf{B}\|\mathbf{Q}$ and $\mathbf{B}\perp\mathbf{Q}$ configurations for the nuclear (006) and (110) reflections also yielded zero net intensity, as expected if there is no ferromagnetic component. The basic spin structure for the low-T phase is shown in Fig. 3(c), which consists of a collinear arrangement of spins with the spin direction in the tetragonal plane.

In the high-T ordered phase, on the other hand, the chain moments are thermally disordered, while the plane moments reorient themselves into a new antiferromagnetic configuration, and we have an ordering sequence like $(+0-+0-\cdots)$ along the c axis. In this case the magnetic and chemical unit cells are the same in this direction, and l will be an integral. We refer to these peaks as the "whole-integral peaks." Two typical magnetic Bragg reflections for this high-T phase that were obtained from the $x=0.1$ crystal at $T=100$ K are shown in Figs. 4(a) and 4(b). The results of the polarized-beam measurements made on the powder sample of $YBa_2Cu_3O_{6.13}$ at $T=200$ K for the $(\frac{1}{2}\ \frac{1}{2}1)$ reflection have been shown in Fig. 1(a) in our previous report,[16] indicating that the whole-integral peaks are also magnetic in origin. Figure 4(c) shows the basic spin structure for the high-T phase.

The temperature dependence of the strongest of these two types of peaks is shown in Figs. 5 and 6 for the $x=0.35$ and $x=0.1$ crystals, respectively. The overall behavior for the two samples is identical, except that their magnetic transition temperatures T_{N1} and T_{N2} are of course different due to their different oxygen contents. No hysteresis was observed in the warming and cooling cycles for any of these magnetic phase transitions.

There are several points to note about these magnetic intensities and their associated order parameters.

(1) In the high-T phase the scattering seems to flatten, or saturate, with decreasing temperature [Figs. 5(a) and 6(a)], indicating that the ordered moment in the plane layers has reached its maximum value. Indeed, in the powder samples that have been studied and in which no chain ordering is observed, no significant increase in intensity at low temperatures has been observed.

(2) The decrease in the intensity of the $(\frac{1}{2}\ \frac{1}{2}\ 2)$ peak at low T is accompanied by the development of intensity at

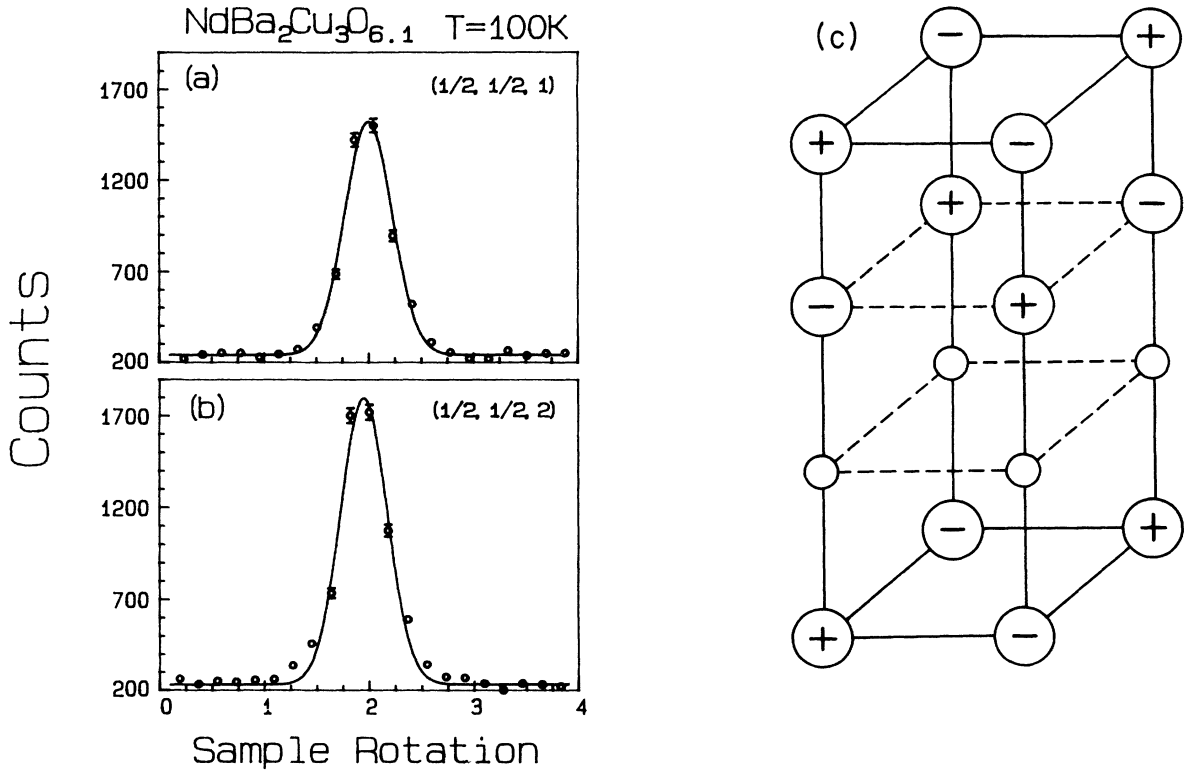

FIG. 4. Two typical magnetic Bragg reflections in the high-T phase. Shown are the $(\frac{1}{2}\,\frac{1}{2}\,1)$ and $(\frac{1}{2}\,\frac{1}{2}\,2)$ reflections from the $x=0.1$ crystal at $T=100$ K. The basic spin structure for the Cu moment at high T is shown in (c). The Cu moments in the oxygen-deficient planes (small circles) are thermally disordered.

the $(\frac{1}{2}\,\frac{1}{2}\,\frac{3}{2})$ peak position. Both changes mark the onset of the "low-T phase" at T_{N2}.

(3) The $(\frac{1}{2}\,\frac{1}{2}\,2)$ intensities appear to extrapolate to zero at $T=0$, indicating that the ground-state magnetic structure (for the Cu spins[35]) includes only half-integral-type peaks.

(4) The intensity of the $(\frac{1}{2}\,\frac{1}{2}\,\frac{3}{2})$ peak is substantially larger than the maximum intensity of the $(\frac{1}{2}\,\frac{1}{2}\,2)$ peak. Indeed our analysis shows that in addition to the ordering of the chain spins, the ordered moment of the plane spins also increases in this low-T phase.

(5) The temperature dependence of the magnetic intensities indicates that $T_{N1}\approx 430$ K and $T_{N2}\approx 80$ K for the $x=0.1$ crystal, and $T_{N1}\approx 230$ K and $T_{N2}\approx 10$ K for the $x=0.35$ crystal.

(6) The intensity for the $(\frac{1}{2}\,\frac{1}{2}\,\frac{3}{2})$ peaks decreases quickly with increasing T, and gives an extrapolated transition temperature as given in (5). However, there is substantial "rounding" to the transition for both crystals as shown in the figures. For example, at 100 K in the $x=0.1$ crystal there is still a sharp peak at the $(\frac{1}{2}\,\frac{1}{2}\,\frac{3}{2})$ position, although it has very weak intensity. This rounding is due either to a distribution of transition temperatures or to an induced moment on the chain sites caused by a coupling to the (ordered) plane sites.

(7) Measurements[14] made on a single crystal of $YBa_2Cu_3O_{6.2}$ show $T_{N1}\approx 400$ K and $T_{N2}\approx 40$ K. These results indicate that *both* T_{N1} and T_{N2} decrease with increasing x in this range of x.

Since the half-integral and whole-integral Bragg reflections correspond to separate Fourier components, they can be treated separately. We may then solve the components of the spin structure for the two types of reflections separately, and then superpose them (vectorially) to obtain the resultant spin structure. We note that the resulting spin structure may be noncollinear. In general the angle between these two components of a spin structure *cannot* be obtained uniquely from the intensity data. However, if we make the physically reasonable assumption that the magnitude of the moments on the two plane layers are the same, then the angle between the two components of the spin structure must be 90° in order to have half-integral and whole-integral peaks completely disappear at high and low temperatures, respectively, and to have these two types of reflections coexist at intermediate temperatures. In addition, a qualitative survey of the observed intensities shows that the spins must lie in the tetragonal plane. There are therefore three adjustable spin parameters that belong to the two vector spins $\mathbf{M}_C$ and $\mathbf{M}_P$, where the subscripts "C" and "P" refer to the

moments of the chain and the plane layers, respectively. One parameter is M_C, the magnitude of the chain moment, and the other two parameters are the components $M_{P\parallel}$ and $M_{P\perp}$, which are parallel and perpendicular, respectively, to the moment direction on the chain layers. We find that at the lowest temperature only M_C and $M_{P\parallel}$ are needed to explain the intensities of the half-integral peaks, so that $M_{P\perp}=0$, while in the high-temperature phase $M_C=M_{P\parallel}=0$ and only $M_{P\perp}$ is needed to explain the intensities of the whole-integral peaks. At intermediate temperatures we have both kinds of peaks, and hence all three parameters are needed. This results in a noncollinear structure. It should also be noted that the direction of $\mathbf{M}_C$ in the tetragonal plane *cannot* be determined from our measurements, since the different domains of the crystals were found to be equally populated, and the information on this direction is lost when a domain average is taken.

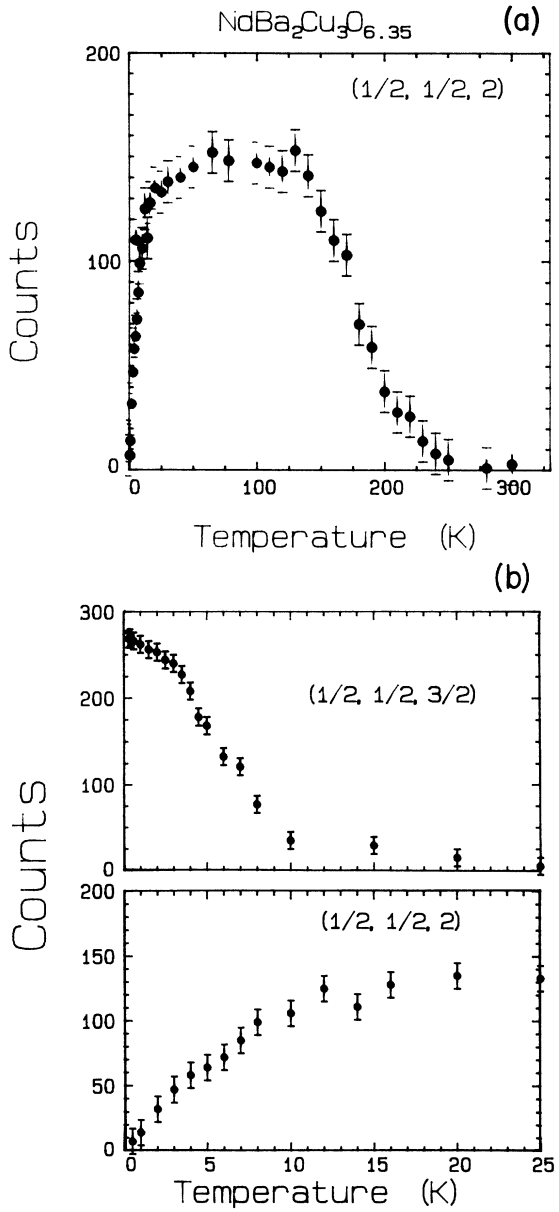

FIG. 5. Temperature dependence of the (net) magnetic intensities for the $NdBa_2Cu_3O_{6.35}$ crystal. The onset of magnetic order for this oxygen concentration is $T_{N1}\approx 230$ K as revealed by the intensity of the $(\frac{1}{2}\,\frac{1}{2}\,2)$ peak shown in (a). The sharp downturn in the $(\frac{1}{2}\,\frac{1}{2}\,2)$ intensity at low temperatures is accompanied by new Bragg peaks at positions such as $(\frac{1}{2}\,\frac{1}{2}\,\frac{3}{2})$ as shown in (b), indicating that the spins are undergoing a change in structure. T_{N2} for this oxygen concentration is ≈ 10 K. Also shown in part (b) is the $(\frac{1}{2}\,\frac{1}{2}\,2)$ intensity on an expanded temperature scale so that it can be directly compared with the $(\frac{1}{2}\,\frac{1}{2}\,\frac{3}{2})$ intensity.

A. High-temperature ordered phase

In the high-temperature ordered phase, when $T_{N2}<T<T_{N1}$, only whole-integral reflections are observed. Some typical whole-integral reflections of the $(\frac{1}{2}\,\frac{3}{2}\,l)$ type taken on the $NdBa_2Cu_3O_{6.1}$ crystal at $T=110$ K are shown in Fig. 7: Reflections of the $(\frac{1}{2}\,\frac{1}{2}\,l)$ type from the $NdBa_2Cu_3O_{6.35}$ crystal at $T=78$ K have already

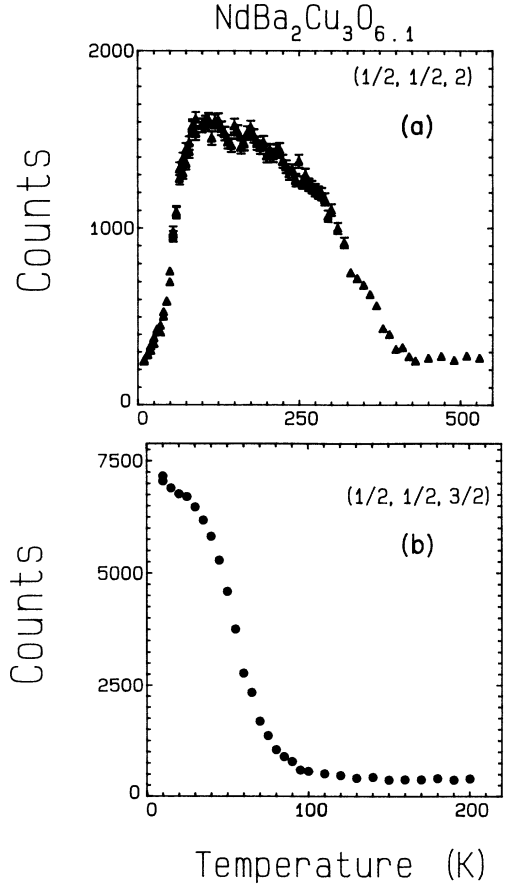

FIG. 6. Temperature dependence of the observed intensities (magnetic Bragg peak plus background) for the $NdBa_2Cu_3O_{6.1}$ crystal. Here the downturn of the $(\frac{1}{2}\,\frac{1}{2}\,2)$ peak begins at much higher temperature. The $(\frac{1}{2}\,\frac{1}{2}\,2)$ intensity at low T is very small, while the $(\frac{1}{2}\,\frac{1}{2}\,\frac{3}{2})$ peak dominates the low-T scattering. At this oxygen concentration $T_{N1}\approx 430$ K and $T_{N2}\approx 80$ K.

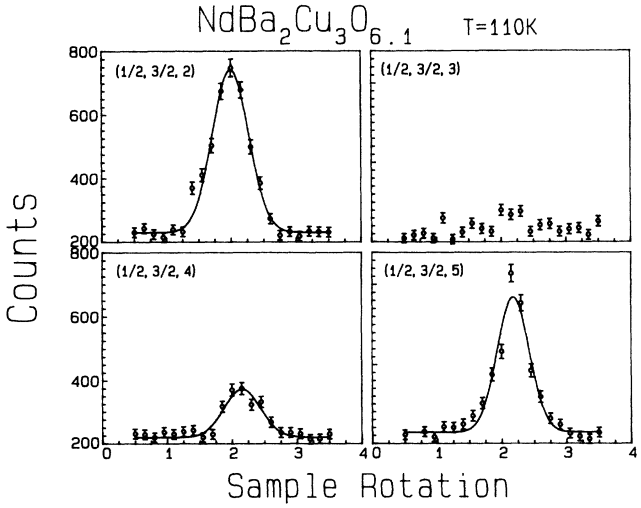

FIG. 7. Several antiferromagnetic whole-integral peaks with $h \neq k$, obtained on the $x=0.1$ crystal at $T=110$ K. The half-integral reflections are unobservable at this temperature, and the solid curves are a least-squares fit to a Gaussian (resolution) function.

been given in Fig. 2 of our previous report.[16] These data were obtained by rotating the crystal through the Bragg peak with the detector set at the Bragg angle. The observed magnetic integrated intensities for the $x=0.1$ crystal at $T=110$ K and for the $x=0.35$ crystal at $T=80$ K are listed in Tables I and II, respectively. The spin structure that we deduce from our data is that the Cu spins in the chain layers are disordered, presumably due to the weaker coupling caused by the reduced amount of oxygen in these layers. The magnetic structure of the plane layers consists of a simple (collinear) antiferromagnetic arrangement of spins both within the planes, and along the tetragonal c axis as shown in Fig. 4(c). The specific spin configurations in each layer are depicted in Fig. 8(a). Within each plane layer we have a collinear $+\mathbf{M}_{P\perp}, -\mathbf{M}_{P\perp}$ arrangement along both directions, while along the c axis we have the (collinear) $+\mathbf{M}_{P\perp}, 0, -\mathbf{M}_{P\perp}$ arrangement. It is important to note in Fig. 8 that we have chosen $\mathbf{M}_{P\perp}$ to be along the a axis for clarity, but in fact this choice is arbitrary, and we do not know the specific direction of $\mathbf{M}_P$ within the plane. This spin arrangement gives rise to whole-integral Bragg reflections only, with the l index integral, since there are two plane layers in the chemical unit cell.

The temperature dependence of the whole-integral peaks has already been shown in Figs. 5(a) and 6(a). In this phase the magnetic intensity is directly proportional to the square of $M_{P\perp}$, which is the sublattice magnetization. The maximum intensity occurs at about 100 K for the $x=0.1$ crystal, and corresponds to a moment of $0.64\pm0.06\mu_B$. We quote the value here that we obtained from our powder data, since extinction effects for the nuclear peaks rendered the single-crystal moment values less reliable. This moment value is in good agreement with values obtained by others.[11,12,15]

TABLE I. Observed and calculated magnetic intensities for the single crystal of $NdBa_2Cu_3O_{6.1}$ with $T_{N1}\approx430$ K and $T_{N2}\approx80$ K. Data were obtained using neutrons of $E_i=14.8$ meV. At $T=110$ K, the half-integral reflections show no intensities. The Cu spins in the chain layers are disordered. In the calculation $M_C=0.00\mu_B$, $M_{P\parallel}=0.00\mu_B$, and $M_{P\perp}=0.64\mu_B$ were used. At $T=100$ K, the scattering is still dominated by the whole-integral peaks. The moments on the chain layers start to develop. In the calculation $M_C=0.09\mu_B$, $M_{P\parallel}=0.21\mu_B$, and $M_{P\perp}=0.63\mu_B$ were used. At $T=20$ K, the half-integral intensities dominate the scattering. In the calculation $M_C=0.32\mu_B$, $M_{P\parallel}=0.78\mu_B$, and $M_{P\perp}=0.28\mu_B$ were used. At $T=10$ K, we have $M_C=0.34\mu_B$, $M_{P\parallel}=0.80\mu_B$, and $M_{P\perp}=0.15\mu_B$.

(hkl)	I_{obs}	I_{calc}
	$T=110$ K	
$(\frac{1}{2}\frac{1}{2}1)$	16.08±1.27	15.78
$(\frac{1}{2}\frac{1}{2}\frac{3}{2})$	<1.1	0.00
$(\frac{1}{2}\frac{1}{2}2)$	26.64±1.56	27.71
$(\frac{1}{2}\frac{1}{2}\frac{5}{2})$	<1.1	0.00
$(\frac{1}{2}\frac{1}{2}5)$	24.70±2.06	29.93
$(\frac{1}{2}\frac{1}{2}\frac{11}{2})$	<1.1	0.00
$(\frac{1}{2}\frac{3}{2}0)$	<1.1	0.00
$(\frac{1}{2}\frac{1}{2}\frac{3}{2})$	<1.1	0.00
$(\frac{1}{2}\frac{3}{2}1)$	11.80±1.26	11.23
$(\frac{1}{2}\frac{3}{2}2)$	20.08±1.92	18.14
$(\frac{1}{2}\frac{3}{2}\frac{5}{2})$	<1.1	0.00
$(\frac{1}{2}\frac{3}{2}3)$	3.61±2.01	3.15
$(\frac{1}{2}\frac{3}{2}\frac{7}{2})$	<1.1	0.00
$(\frac{1}{2}\frac{3}{2}4)$	6.13±1.66	4.73
$(\frac{1}{2}\frac{3}{2}\frac{9}{2})$	<1.1	0.00
$(\frac{1}{2}\frac{3}{2}5)$	16.36±1.92	17.25
$(\frac{1}{2}\frac{3}{2}\frac{11}{2})$	<1.1	0.00
	$T=100$ K	
$(\frac{1}{2}\frac{1}{2}1)$	15.93±1.02	15.02
$(\frac{1}{2}\frac{1}{2}\frac{3}{2})$	4.18±0.39	4.17
$(\frac{1}{2}\frac{1}{2}2)$	25.89±1.83	26.38
$(\frac{1}{2}\frac{1}{2}\frac{5}{2})$	0.93±0.35	0.93
$(\frac{1}{2}\frac{1}{2}3)$	4.46±0.36	4.53
$(\frac{1}{2}\frac{1}{2}4)$	8.08±1.13	7.16
$(\frac{1}{2}\frac{1}{2}5)$	29.26±1.51	28.47
$(\frac{1}{2}\frac{1}{2}6)$	11.58±0.89	12.34
$(\frac{3}{2}\frac{3}{2}2)$	8.66±1.93	11.85
	$T=20$ K	
$(\frac{1}{2}\frac{1}{2}\frac{3}{2})$	73.51±2.81	75.73
$(\frac{1}{2}\frac{1}{2}2)$	4.86±1.62	7.03
$(\frac{1}{2}\frac{3}{2}0)$	<1.1	0.00
$(\frac{1}{2}\frac{3}{2}\frac{1}{2})$	1.79±1.18	1.73
$(\frac{1}{2}\frac{3}{2}1)$	3.17±1.34	2.85

TABLE I. (*Continued*).

(*hkl*)	I_{obs}	I_{calc}
	$T=20$ K	
$(\frac{1}{2}\ \frac{3}{2}\ 2)$	4.82±1.72	4.60
$(\frac{1}{2}\ \frac{3}{2}\ \frac{5}{2})$	10.44±1.82	11.44
$(\frac{1}{2}\ \frac{3}{2}\ 3)$	<1.1	0.80
$(\frac{1}{2}\ \frac{3}{2}\ \frac{7}{2})$	<1.1	0.97
$(\frac{1}{2}\ \frac{3}{2}\ 4)$	<1.1	1.20
$(\frac{1}{2}\ \frac{3}{2}\ \frac{9}{2})$	40.85±1.58	38.81
$(\frac{1}{2}\ \frac{3}{2}\ 5)$	4.34±1.14	4.38
$(\frac{1}{2}\ \frac{3}{2}\ \frac{11}{2})$	18.01±2.28	17.12
	$T=10$ K	
$(\frac{1}{2}\ \frac{1}{2}\ \frac{1}{2})$	2.47±0.30	2.38
$(\frac{1}{2}\ \frac{1}{2}\ 1)$	1.87±0.53	1.21
$(\frac{1}{2}\ \frac{1}{2}\ \frac{3}{2})$	82.80±3.20	81.86
$(\frac{1}{2}\ \frac{1}{2}\ 2)$	1.93±0.51	2.12
$(\frac{1}{2}\ \frac{1}{2}\ \frac{5}{2})$	19.34±1.14	18.51
$(\frac{1}{2}\ \frac{1}{2}\ 3)$	<0.7	0.36
$(\frac{1}{2}\ \frac{1}{2}\ \frac{7}{2})$	1.35±0.45	1.67
$(\frac{1}{2}\ \frac{1}{2}\ 4)$	<0.7	0.58
$(\frac{1}{2}\ \frac{1}{2}\ 5)$	2.30±0.77	2.29
$(\frac{1}{2}\ \frac{1}{2}\ \frac{11}{2})$	28.45±1.35	31.31
$(\frac{1}{2}\ \frac{1}{2}\ 6)$	0.99±0.37	0.99
$(\frac{3}{2}\ \frac{3}{2}\ \frac{1}{2})$	1.58±0.45	1.38
$(\frac{3}{2}\ \frac{3}{2}\ 1)$	<0.7	0.64
$(\frac{3}{2}\ \frac{3}{2}\ \frac{3}{2})$	39.14±3.17	39.38
$(\frac{3}{2}\ \frac{3}{2}\ 2)$	1.29±0.61	0.95
$(\frac{3}{2}\ \frac{3}{2}\ \frac{5}{2})$	6.05±1.89	7.95
$(\frac{3}{2}\ \frac{3}{2}\ 3)$	<0.7	0.15

B. Ground state

With a further decrease in temperature, a second phase transition at T_{N2} occurs as shown in Figs. 5 and 6. New peaks appear at positions with l half integral, which implies that the magnetic unit cell has now doubled along the c axis as well as in the tetragonal plane. Accompanied by the increase in the intensities of these half-integral peaks is a decrease in the whole-integral peaks, and in fact these intensities appear to extrapolate to zero at $T=0$. We therefore assume that the ground-state spin configuration of the system corresponds to Bragg reflections in which all three Miller's indices are half integers. The spin structure we have determined is shown in Fig. 3(c), in which both the plane and the chain layers carry ordered Cu moments, with a simple collinear antiferromagnetic $+-+-+-$ arrangement along all three crystallographic directions. The spin arrangements are shown in more detail in Fig. 8(b), where we have a collinear stacking of $-\mathbf{M}_{P\parallel}, +\mathbf{M}_C, -\mathbf{M}_{P\parallel}+\mathbf{M}_{P\parallel}, -\mathbf{M}_C, +\mathbf{M}_{P\parallel}$ along the c axis, and a collinear arrangement of $+\mathbf{M}_{P\parallel}, -\mathbf{M}_{P\parallel}$ and $+\mathbf{M}_C, -\mathbf{M}_C$ along both directions in the tetragonal plane and the chain layers, respectively.

The values of the ordered moments that we obtained at

TABLE II. Observed and calculated magnetic intensities for the single crystal of $NdBa_2Cu_3O_{6.35}$ with $T_{N1}\approx 230$ K and $T_{N2}\approx 10$ K. At $T=80$ K, only the whole-integral peaks were observed at this temperature. $M_C=0.0\mu_B$, $M_{P\parallel}=0.0\mu_B$, and $M_{P\perp}=0.64\mu_B$ were used in the calculation. Data were obtained using neutrons of $E_i=28.3$ meV. At $T=5$ K, both half-integral and whole-integral peaks were observed. $M_C=0.23\mu_B$, $M_{P\parallel}=0.14\mu_B$, and $M_{P\perp}=0.23\mu_B$ were used. Data were obtained using neutrons of $E_i=14.8$ meV.

(*hkl*)	I_{obs}	I_{calc}
	$T=80$ K	
$(00\frac{1}{2})$	<1.5	0.00
$(00\frac{3}{2})$	<1.5	0.00
$(\frac{1}{2}\ \frac{1}{2}\ 0)$	<1.5	0.00
$(\frac{1}{2}\ \frac{1}{2}\ 1)$	11.25±1.42	9.95
$(\frac{1}{2}\ \frac{1}{2}\ 2)$	16.39±2.08	17.33
$(\frac{1}{2}\ \frac{1}{2}\ 3)$	2.49±1.74	2.93
$(\frac{1}{2}\ \frac{1}{2}\ 4)$	4.96±1.84	4.53
$(\frac{1}{2}\ \frac{1}{2}\ 5)$	15.58±2.59	17.42
$(\frac{1}{2}\ \frac{1}{2}\ 6)$	7.32±2.08	7.15
$(\frac{1}{2}\ \frac{1}{2}\ 7)$	<1.5	0.12
$(\frac{1}{2}\ \frac{1}{2}\ 8)$	6.76±2.29	6.02
$(\frac{1}{2}\ \frac{1}{2}\ 9)$	6.27±1.40	5.82
$(\frac{1}{2}\ \frac{1}{2}\ 10)$	<1.5	0.43
$(\frac{3}{2}\ \frac{3}{2}\ 0)$	<1.5	0.00
$(\frac{3}{2}\ \frac{3}{2}\ 1)$	4.11±1.95	4.59
$(\frac{3}{2}\ \frac{3}{2}\ 2)$	2.30±1.39	6.74
$(\frac{3}{2}\ \frac{3}{2}\ 3)$	<1.5	1.04
$(\frac{3}{2}\ \frac{3}{2}\ 4)$	<1.5	1.54
$(\frac{3}{2}\ \frac{3}{2}\ 5)$	5.62±2.65	5.99
$(\frac{3}{2}\ \frac{3}{2}\ 6)$	2.95±1.38	2.92
$(\frac{3}{2}\ \frac{3}{2}\ 7)$	<1.5	0.06
$(\frac{3}{2}\ \frac{3}{2}\ 8)$	3.40±1.42	3.18
$(\frac{3}{2}\ \frac{3}{2}\ 9)$	2.57±1.40	3.15
$(\frac{5}{2}\ \frac{5}{2}\ 1)$	<1.5	1.52
$(\frac{5}{2}\ \frac{5}{2}\ 2)$	<1.5	2.24
$(\frac{5}{2}\ \frac{5}{2}\ 3)$	<1.5	0.36
	$T=5$ K	
$(\frac{1}{2}\ \frac{1}{2}\ 1)$	2.59±0.43	2.48
$(\frac{1}{2}\ \frac{1}{2}\ \frac{3}{2})$	5.03±0.50	5.15
$(\frac{1}{2}\ \frac{1}{2}\ 2)$	4.42±0.53	4.35
$(\frac{1}{2}\ \frac{1}{2}\ 5)$	4.56±0.83	4.69
$(\frac{3}{2}\ \frac{3}{2}\ 1)$	1.51±0.86	1.31

low temperatures are $M_{P\parallel}=0.81\pm0.08\mu_B$ for the plane layers and $M_C=0.35\pm0.06\mu_B$ for the chain layers, with $M_{P\perp}=0$, since the spin configuration is collinear. Note that the value of the ordered moment in the planes is now substantially larger than the maximum moment obtained when only the plane moments are ordered, above T_{N2}.

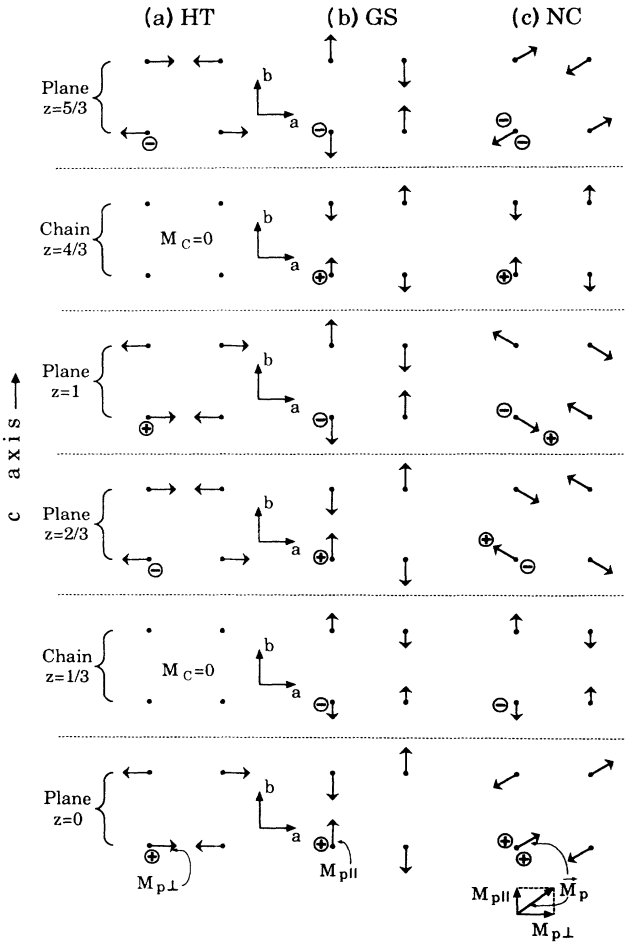

FIG. 8. A sequence of six layers of Cu spins is shown. At all temperatures, when there are ordered moments on the Cu ions, the spins have a simple antiferromagnetic arrangement of nearest neighbors along both directions in the tetragonal planes as shown, with the spin direction in the tetragonal plane. $\mathbf{M}_C$ is the moment on the chain layers, $\mathbf{M}_{P\parallel}$ and $\mathbf{M}_{P\perp}$ are the moments on the plane layers that are $\parallel$ and $\perp$, respectively, to $\mathbf{M}_C$. In the high-temperature ordered phase, $\mathbf{M}_C=\mathbf{M}_{P\parallel}=0$, only the plane layers are ordered, and the spin structure is collinear as shown in (a), and the $(+-)$ sequence along the c axis is the same as shown in Fig. 4(c). At $T\approx0$, $\mathbf{M}_{P\perp}=0$, $\mathbf{M}_C\approx0.43\mathbf{M}_{P\parallel}$, and the spin structure is again collinear as shown in (b), with the $(+-)$ the same as that shown in Fig. 3(c). The spin configuration at intermediate temperatures is a (vector) superposition of (a) and (b), which yields a noncollinear structure as shown in (c). As the temperature is raised from $T=0$, the values for $M_{P\parallel}$ and M_C decrease while that for $M_{P\perp}$ increases as the spins in the plane layers rotate. The specific direction of $\mathbf{M}_C$ within the tetragonal plane *cannot* be determined from our measurements, and we have simply chosen it to be along one of the axes for clarity.

We remark that in some samples no chain ordering has been observed, i.e., $T_{N2}\rightarrow0$, and then the increased plane moment is not observed. The reduced value of the Cu moment in the planes has been interpreted as resulting from the large spin fluctuations originating from the 2D behavior of the planes, and the increased moment we observe when the chains order adds further credence to this interpretation.

C. Intermediate temperatures

The exchange interactions between layers are shown schematically in Fig. 9. In the high-T phase, when the chains are thermally disordered, the planes are coupled antiferromagnetically, and hence we take $J_{p1}<0$ and $J_{p2}<0$, where J_{p1} is the interaction between adjacent planes, and J_{p2} is the interaction between planes which is mediated through the chain layer. Note that J_{p2} is really a next-nearest-neighbor interaction, and hence we can assume that J_{p2} is a weaker interaction than J_{p1}. Of course, the exchange interactions within the CuO_2 layers are also antiferromagnetic, and are much stronger than any of these interactions between layers.

When the chain moments order, we must introduce another exchange interaction J_{pc}, which is the (nearest-neighbor) interaction between adjacent chain and plane layers. Note that J_{p2} and J_{pc} cannot be satisfied simultaneously, and hence we have a situation of competing interactions. The observed ground-state configuration then establishes that J_{pc} is stronger than J_{p2}.

The result of these competing interactions is that the spin structure becomes noncollinear. Just below T_{N2}, the moments on the chains point in a direction perpendicular to the moments in the planes. As the temperature is lowered, M_C increases in magnitude, and the moments on the planes rotate toward the direction of $\mathbf{M}_C$ and finally become antiparallel to $\mathbf{M}_C$ in the ground-state configuration.

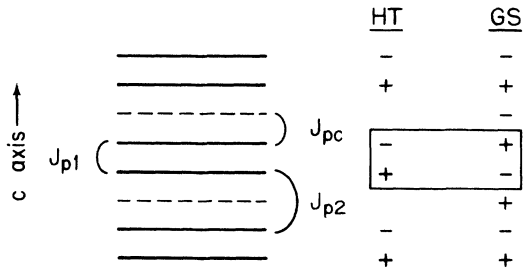

FIG. 9. Schematic of the exchange interactions along the c axis. J_{p1} is the direct interaction between plane layers, and J_{p2} is the interaction between plane layers that is mediated through the (thermally disordered) chain layers. J_{pc} is the direct interaction between the chain and plane layers when the chains are ordered. All three interactions are antiferromagnetic.

D. Quantitative analysis

In the intermediate temperature regime, where $0 < T < T_{N2}$, both whole-integral and half-integral peaks are observed, and the spin configuration is noncollinear as shown in Fig. 8(c). Figure 10 shows examples of both the $(\frac{1}{2}\,\frac{1}{2}\,l)$ and $(\frac{1}{2}\,\frac{1}{2}\,l/2)$ Bragg reflections observed at $T=100$ K from the $x=0.1$ crystal. Note that the y scale for the whole-integral reflections is twice that for the half-integral reflections, and the whole-integral reflections obviously dominate the scattering at this temperature. At low temperature, on the other hand, the reverse is true and the half-integral reflections dominate. Some typical data are shown in Fig. 11. In particular, note that a ratio of 4:2:1 for the integrated intensities of the $(\frac{1}{2}\,\frac{1}{2}\,\frac{3}{2})$ and $(\frac{1}{2}\,\frac{1}{2}\,\frac{5}{2})$ reflections is observed, which is an important key for us to obtain the spin structure at low temperatures. The observed magnetic integrated intensities for the $x=0.1$ crystal at three different temperatures are listed in the second, third, and fourth parts of Table I, while those for the $x=0.35$ crystal at $T=5$ K are listed in the second part of Table II.

As the temperature is decreased, $M_{P\perp}$ decreases, while both M_C and $M_{P\parallel}$ increase. The spin structure along the c axis is then the superposition of two orthogonal collinear stackings of $+\mathbf{M}_{P\perp}, 0, -\mathbf{M}_{P\perp}, +\mathbf{M}_{P\perp}, 0, -\mathbf{M}_{P\perp}$ and $-\mathbf{M}_{P\parallel}, +\mathbf{M}_C, -\mathbf{M}_{P\parallel}, +\mathbf{M}_{P\parallel}, -\mathbf{M}_C, +\mathbf{M}_{P\parallel}$. These stackings are indicated in Figs. 8(a) and 8(b) by the $\oplus$ and $\ominus$. The resultant noncollinear structure is shown in Fig. 8(c). Along both directions in the tetragonal planes, the structure remains a collinear arrangement of $+\mathbf{M}_P, -\mathbf{M}_P$ and $+\mathbf{M}_C, -\mathbf{M}_C$ in the plane and chain layers, respectively.

It turns out that the relative intensities between the half-integral reflections do not depend on the value of $M_{P\perp}$, which allows us to determine the best value for $M_C/M_{P\parallel}$ by using all of the observed half-integral intensities. Once $M_C/M_{P\parallel}$ is known, $M_{P\perp}/M_{P\parallel}$ can then be determined by using the observed relative intensities between the half-integral and whole-integral peaks. Finally, the value of $M_{P\parallel}$ is obtained by detailed comparisons[16] of the whole-integral intensities with the nuclear intensities. The values for M_C, $M_{P\parallel}$, and $M_{P\perp}$ thus obtained for the $x=0.1$ and $x=0.35$ crystals at various temperatures are listed in Tables I and II, respectively, where comparisons of the observed and calculated magnetic Bragg intensities are also shown. The agreement between the data and the model calculation is quite good. In the calculation, magnetic form factors measured[36] for Cu^{2+} in ferromagnetic K_2CuF_4 were used, the angular (Lorentz) factors for a single crystal were considered, and the calculated intensities were averaged over all possible domains.

The relative intensities between the half-integral reflections depend on the relative moment of the Cu ions on the chain and plane layers, i.e., they depend on $M_C/M_{P\parallel}$. We observed a much stronger $(\frac{1}{2}\,\frac{1}{2}\,\frac{3}{2})$ reflection than other reflections like $(\frac{1}{2}\,\frac{1}{2}\,\frac{5}{2})$ and $(\frac{3}{2}\,\frac{3}{2}\,\frac{3}{2})$, and a relative moment of $M_C/M_{P\parallel} \approx 0.43$ is deduced from our data taken on the $x=0.1$ crystal at $T=10$ K. The

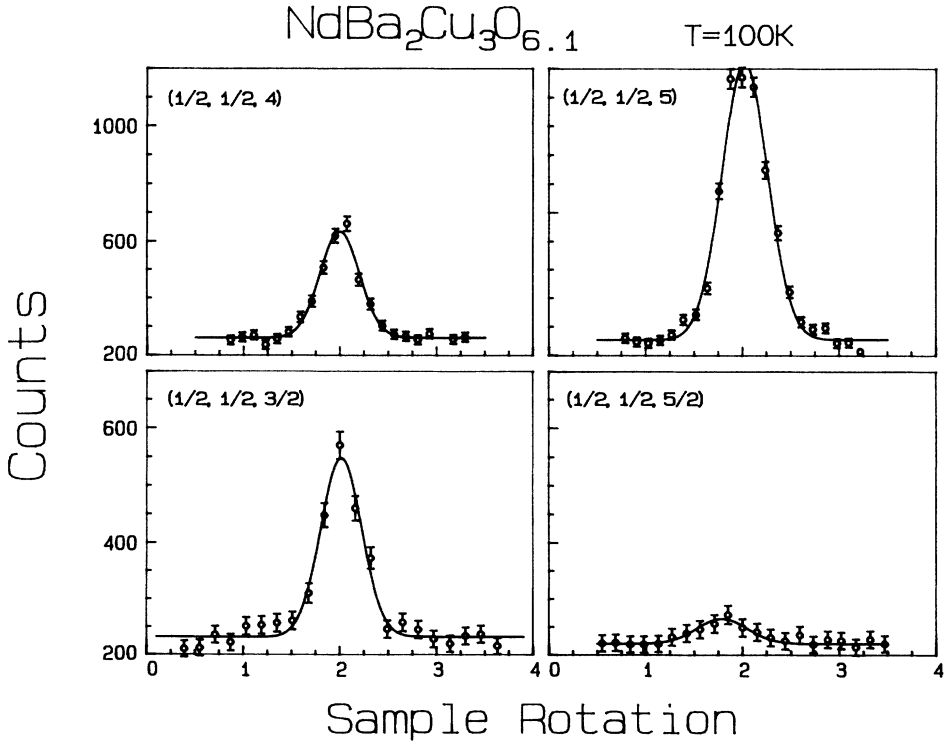

FIG. 10. These data were obtained on the $x=0.1$ crystal at $T=100$ K, where both half-integral and whole-integral peaks have nonzero intensities. Note that the intensity scale for the whole-integral peaks is twice that for the half-integral peaks.

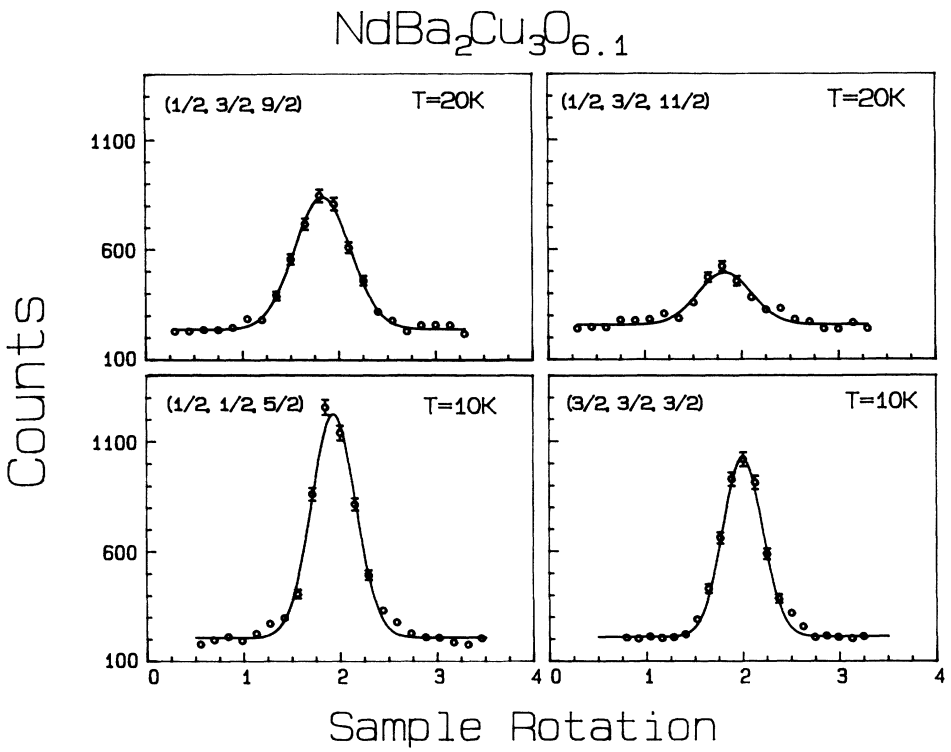

FIG. 11. Several half-integral peaks obtained with the $x=0.1$ crystal at low temperatures.

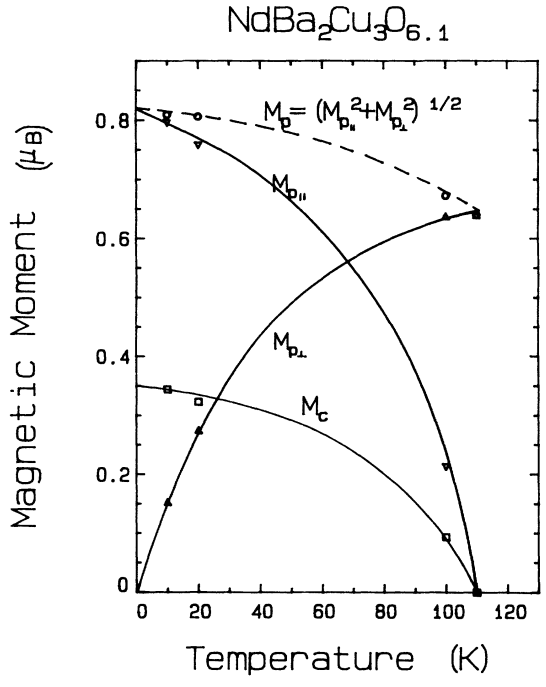

FIG. 12. Temperature dependence of the ordered moment on the Cu ions for the $x=0.1$ crystal. At low temperatures, the moment on the chain layers is about 40% of that on the plane layers. As $T \rightarrow T_{N2}$, M_C drops to zero, and only the spins on the Cu in the plane layers remain ordered. The solid curves are a guide to the eye.

values of the ordered moments that we obtained at low temperatures are then $M_P=(0.81\pm0.08)\mu_B$ for the plane layers and $M_C=(0.35\pm0.06)\mu_B$ for the chain layers. The temperature dependence of the moments on the Cu ions for the $x=0.1$ crystal is shown in Fig. 12. The relatively large moment observed in the chain layers is somewhat surprising. As the temperature is raised, the thermal agitation randomizes these spins, resulting in a reduction of the average moments: Both M_C and M_P decrease with increasing temperature, with M_C decreasing faster than M_P does. As the temperature reaches T_{N2}, M_C drops to zero signifying that the Cu spins in the chain layers become completely disordered, while a moment as high as $0.65\mu_B$ still remains on the Cu ions in the plane layers.

IV. MAGNETIC-FIELD DEPENDENCE

A few exploratory measurements were made on the field dependence of the magnetic Bragg intensities to determine the qualitative effect of an applied field on the magnetic system. The data were restricted to low temperatures (5 K), and were taken in a superconducting magnet with a field range from zero to 7 T. The crystal was mounted in the (hhl) scattering plane, with the field applied vertically, that is, in the $[h\bar{h}0]$ direction. Hence the field was applied in the (easy) tetragonal plane.

For an antiferromagnet in an applied field we can expect two basic kinds of behavior, depending on the relative strengths of the anisotropy and exchange.[37] Consider the situation where B is applied along the spin axis. If

the anisotropy dominates, then we will have a metamagnetic transition at a certain critical field B_M, where the sublattice that opposes the field suddenly changes direction by 180° and all the spins become parallel. This costs the full exchange energy of the system, but costs no anisotropy energy. If, on the other hand, the exchange energy dominates, which is surely the case in these oxide systems where the intraplanar exchange energies are huge, then we will have a spin-flop (SF) transition at a critical field B_{SF}, where the spins maintain their basic antiparallel arrangement but both sublattices rotate by $\sim 90°$ so that the spins are essentially perpendicular to B. There is also a small canting of the spins in the direction of B, which yields a small (induced) ferromagnetic component. Then, with further increase of field the spins will cant further to become better aligned with B. At sufficiently high B, when the dipolar energies dominate the energetics, again the spins will all become parallel. In the present case, however, where the exchange energies are very large, such fields will not be experimentally accessible. Finally, with tetragonal symmetry we will need to consider the case where B is applied perpendicular to the initial ($B=0$) spin direction. This is the same as the spin-flip case just discussed, with $B > B_{SF}$.

The peak intensities versus field were measured at 5 K for the $(\frac{1}{2}\,\frac{1}{2}\,2)$ and $(\frac{1}{2}\,\frac{1}{2}\,\frac{3}{2})$ antiferromagnetic peaks, as well as for several nuclear peaks where we checked for an induced ferromagnetic component. No ferromagnetic component was observed at any field, indicating that the dipolar energies are indeed small compared to the exchange energies as already discussed. The intensities of the antiferromagnet peaks, on the other hand, are quite sensitive to B as shown in Fig. 13, where a decrease of the net intensity of $\sim 20\%$ is observed up to 6 T. A similar decrease was observed for the $(\frac{1}{2}\,\frac{1}{2}\,2)$ peak, although at this low temperature the even-integer peaks have quite small intensities and hence the statistics are not nearly as good.

The data of Fig. 13 can be interpreted in a straightforward way assuming that the exchange energies dominate. At 5 K we are in the low-temperature phase, where all the Cu layers are ordered in a collinear spin arrangement as shown in Fig. 8(b). In this case Eq. (2) can be written in the usual form[33]

$$\Omega = \left| \sum_j \langle \mu_j^\alpha \rangle f_j(\mathbf{K}) e^{i\mathbf{K}\cdot\mathbf{r}_j} \right|^2 \langle 1-(\hat{\tau}\cdot\hat{\mathbf{M}})^2 \rangle \ , \qquad (4)$$

where we have neglected the Debye-Waller factor at these low temperatures. The term of interest here is the so-called orientation factor $\langle 1-(\hat{\tau}\cdot\hat{\mathbf{M}})^2 \rangle$, where $\hat{\mathbf{M}}$ is a unit vector which defines the spin axis, and $\langle \cdots \rangle$ denotes an average over all possible domain configurations. If we assume, for example, that the $\langle 110 \rangle$ direction is the easy axis for the system, then for domains where $\hat{\mathbf{M}}$ is along $[h\bar{h}0]$ the spins will rotate so that they are in the $[hh0]$ direction, and hence in the scattering plane. The orientation factor will then decrease from its maximum value of 1, to $\frac{1}{3}$, and hence the observed intensity will decrease. For domains where the spin direction is already in the $[hh0]$ direction, the orientation factor will already be $\frac{1}{3}$ and will not change significantly. Hence the total intensity decrease[38] in the vicinity of the spin-flop[39] transition could be as large as a factor of 2. The substantial intensity decrease that is observed indicates that the anisotropy in the tetragonal plane is comparable to the dipolar energies produced by the field, and hence the anisotropy must be very small compared to the exchange energies.

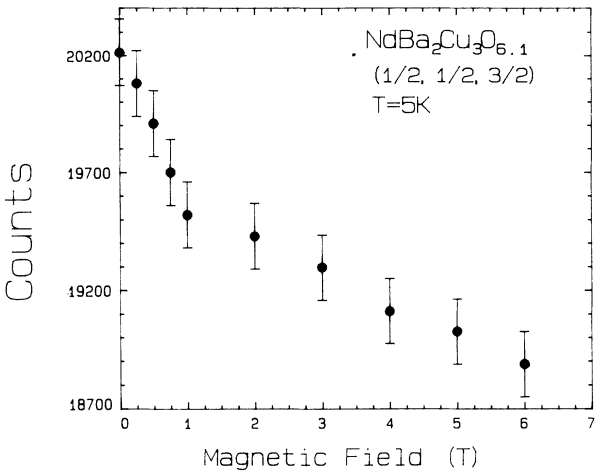

FIG. 13. The magnetic field dependence of the $(\frac{1}{2}\,\frac{1}{2}\,\frac{3}{2})$ peak intensity from the $x=0.1$ crystal at $T=10$ K. The magnetic field was applied in the tetragonal plane.

V. DISCUSSION

The intensities of the ~ 40 independent magnetic reflections that we observed on the single crystals of $NdBa_2Cu_3O_{6.1}$ and $NdBa_2Cu_3O_{6.35}$ are well explained by the assumption of a $3d$ magnetic form factor on the Cu ions with no need for a significant moment on any of the oxygen ions. Polarized beam measurements on $YBa_2Cu_3O_{6.3}$ also have revealed no evidence of a magnetic moment on the oxygen ions.[23] However, it is the oxygen ions that mediate the strong exchange interactions within the Cu-O layers, and produce the 2D like electron correlations which are the genesis of the very high three-dimensional magnetic ordering temperature, and perhaps the high superconducting transition temperature as well. However, even if magnetism is not directly associated with the superconducting state, it is quite clear that the Cu layers are intimately involved in both the magnetism and superconductivity, and the oxygen plays a determinative role in the system.

The principal results of this paper are a detailed understanding of the nature of the magnetic structures and ordering which involve the Cu plane and chain layers. The essential difference between the low-T and high-T spin structures is of course the moment M_C on the chain layers, which develops below T_{N2}. The conventional viewpoint for the $\mathcal{R}Ba_2Cu_3O_{6+x}$ class of materials was that the Cu valence in the plane layers is 2+ with an associated magnetic moment, while the chain layers only

contain nonmagnetic Cu^+ at $x=0$. The incorporation of oxygen into the chain layers then creates some Cu^{2+}, with an average moment on the chains that is very small. This picture was supported by the results of Kadowaki, *et al.*,[14] who reported a very small chain moment. However, they did not measure the half-integral and whole-integral peaks very far below T_{N2}, and they obtained a very limited set of Bragg intensities. Hence they did not realize that the structure is noncollinear in this temperature range, and analyzed their data employing an incorrect spin structure. The small chain moment they quote is not indicative of the full ordered moment.[40] The unexpectedly large value of M_C which we have observed on the Cu chain layers demonstrates that the Cu^+ state is not an appropriate description of the electronic configuration of the chain layers in these materials: There must be strong hybridization of the (band) electronic wave functions within all three Cu layers, and this hybridization is at the origin of the strong electron correlations.

In the present $\mathcal{R}Ba_2Cu_3O_{6+x}$ system, however, the chain ordering has only been observed in some samples and not in others. A central question to address then, is what physical properties control the magnetic moment and ordering on the chain ions, in addition to the average oxygen concentration x. In particular, is the chain ordering a general phenomenon for all the $\mathcal{R}Ba_2Cu_3O_{6+x}$ materials, or it is specific to $NdBa_2Cu_3O_{6+x}$? In this regard it is important to note that the chain ordering is quite sensitive to changes of the electronic structure, either by chemical substitution directly on the chain sites, or elsewhere in the system. The case of Co substitution has been studied in some detail.[41,42] The Co substitutes preferentially on the Cu chain sites, and indeed increasing the Co concentration is found to strongly enhance the chain-ordering temperature T_{N2} until the chains order at the same temperature as the planes. Another example of electronic alteration of the system is provided by Nd substitution on the Ba site. Nd has a relatively large ionic radius, and under some sample preparation conditions can substitute onto the Ba site, yielding $NdBa_{2-y}Nd_yCu_3O_{6+x}$. This changes the electronic configuration of the system, and can affect both the magnetic and superconducting properties.[43] In fact, recently Moudden, *et al.*[13] have reported measurements on a single crystal of nominal composition $NdBa_2Cu_3O_{6+x}$, where they found that the planes and chains order at the same temperature of 385 K. This behavior is quite similar to the situation of Co substitution, and we attribute the high chain-ordering temperature to the electronic changes caused by Nd substituted on the Ba site. Hence the magnetic properties of the chains appear to be strongly influenced by substitutions on either the Cu chain sites or the Ba sites.

The measurements which bare most directly on this point are those of Kadowaki *et al.*,[14] where they observed $T_{N1}=400$ K and $T_{N2}=40$ K on a single crystal of $YBa_2Cu_3O_{6+x}$. These values fall just between our values of (430, 80) and (230, 10) for T_{N1} and T_{N2}, respectively. In addition, the temperature dependence of the half-integral and whole-integral peaks for our samples is identical to their data where they overlap.[40] Hence we conclude that the chain ordering is a general phenomenon for this system, and is not specific to $\mathcal{R}=$Nd. In the case of the single crystal studied by Moudden *et al.*,[13] the sample was prepared by a different growth technique than our crystals, and we think it is likely that the high chain-ordering temperature in their case is indeed due to an occupancy of Nd on the Ba site. We note that the RBS measurements on our own samples revealed no significant Nd on the Ba site.

The final question to address is why the chain ordering is observed in some samples, and not in others. In particular, it has been observed in "as-grown" single crystals, but has not been observed in pure (i.e., not with Co substitution) powders. In single crystals where the oxygen is driven in and out, on the other hand, only suggestions of chain ordering have been observed.[15] We speculate that this chain-ordering behavior is being controlled not only by the oxygen concentration, but also by atomic ordering of the oxygen in the chains.[44] In powders which are quenched relatively quickly, the oxygen occupancy in the b-axis sites is likely random, while in single crystals which are grown slowly there may be a substantial amount of preferred occupancy.[45] Indeed oxygen ordering is believed to be responsible for the "plateau" near $x\sim\frac{2}{3}$ in the superconducting T_c. We also note that Co substitution on the chains may enhance this oxygen ordering, which would help explain the enhanced chain ordering in that case. It is very difficult, however, to observe this chain order in bulk samples, and it is clear that a systematic investigation of the chain ordering as a function of oxygen concentration and atomic ordering will be needed to determine if this speculation has any basis in reality.

ACKNOWLEDGMENTS

We would like to thank R. A. Ferrell, M. E. Fisher, H. A. Mook, and B. C. Sales for helpful discussions and assistance. The research at the University of Maryland was supported by the National Science Foundation (NSF) Grant No. DMR 86-20269 and DMR 89-21878. The Research at Los Alamos National Laboratory was supported by the U.S. Department of Energy.

[1]Y. J. Uemura, W. J. Kossler, X. H. Yu, J. R. Kempton, H. E. Schone, D. Opie, C. E. Stronach, D. C. Johnston, M. S. Alvarez, and D. P. Goshorn, Phys. Rev. Lett. **59**, 1045 (1987).

[2]D. R. Harshman, G. Aeppli, G. P. Espinosa, A. S. Cooper, J. P. Remeika, E. J. Ansaldo, T. M. Riseman, D. L. Williams, D. R. Noakes, B. Ellman, and T. F. Rosenbaum, Phys. Rev. B **38**, 852 (1988); N. Nishida *et al.*, Jpn. J. Appl. Phys. **26**, L1856 (1987); J. Phys. Soc. Jpn. **57**, 722 (1988).

[3]D. Vaknin, S. K. Sinha, D. E. Moncton, D. C. Johnston, J. M. Newsam, C. R. Safinya, and H. E. King, Jr., Phys. Rev. Lett.

58, 2802 (1987).

[4]S. Mitsuda, G. Shirane, S. K. Sinha, D. C. Johnston, M. S. Alvarez, D. Vaknin, and D. E. Moncton, Phys. Rev. B **36**, 822 (1987).

[5]T. Freltoft, J. E. Fischer, G. Shirane, D. E. Moncton, S. K. Sinha, D. Vaknin, J. P. Remeika, A. S. Cooper, and D. Harshman, Phys. Rev. B **36**, 826 (1987).

[6]G. Shirane, Y. Endoh, R. J. Birgeneau, M. A. Kastner, Y. Hidaka, M. Oda, M. Suzuki, and T. Murakami, Phys. Rev. Lett. **59**, 1613 (1987).

[7]T. Freltoft, G. Shirane, S. Mitsuda, J. P. Remeika, and A. S. Cooper, Phys. Rev. B **37**, 137 (1988).

[8]C. Stassis, B. N. Harmon, T. Freltoft, G. Shirane, S. K. Sinha, K. Yamada, Y. Endoh, Y. Hidaka, and T. Murakami, Phys. Rev. B **38**, 9291 (1988).

[9]M. A. Kastner, R. J. Birgeneau, T. R. Thurston, P. J. Picone, H. P. Jenssen, D. R. Gabbe, M. Sato, K. Fukuda, S. Shamoto, Y. Endoh, K. Yamada, and G. Shirane, Phys. Rev. B **38**, 6636 (1988).

[10]Y. Endoh, K. Yamada, R. J. Birgeneau, D. R. Gabbe, H. P. Jenssen, M. A. Kastner, C. J. Peters, P. J. Picone, T. R. Thurston, J. M. Tranquada, G. Shirane, Y. Hidaka, M. Oda, Y. Enomoto, M. Suzuki, and T. Murakami, Phys. Rev. B **37**, 7443 (1988).

[11]J. M. Tranquada, D. E. Cox, W. Kunnmann, H. Moudden, G. Shirane, M. Suenaga, P. Zolliker, D. Vaknin, S. K. Sinha, M. S. Alvarez, A. J. Jacobson, and D. C. Johnston, Phys. Rev. Lett. **60**, 156 (1988).

[12]J. M. Tranquada, A. H. Moudden, A. I. Goldman, P. Zolliker, D. E. Cox, G. Shirane, S. K. Sinha, D. Vaknin, D. C. Johnston, M. S. Alvarez, and A. J. Jacobson, Phys. Rev. B **38**, 2477 (1988).

[13]A. H. Moudden, G. Shirane, J. M. Tranquada, R. J. Birgeneau, Y. Endoh, K. Yamada, Y. Hidaka, and T. Murakami, Phys. Rev. B **38**, 8893 (1988).

[14]H. Kadowaki, M. Nishi, Y. Yamada, H. Takeya, H. Takei, S. Shapiro, and G. Shirane, Phys. Rev. B **37**, 7932 (1988).

[15]P. Burlet, C. Vettier, M. J. G. M. Jurgens, J. Y. Henry, J. Rossat-Mignod, H. Noel, M. Potel, P. Gougeon, and J. C. Levet, Physica **153-155C**, 1115 (1988); D. Petitgrand and G. Collin, *ibid.* **153-155C**, 192 (1988).

[16]W-H. Li, J. W. Lynn, H. A. Mook, and B. C. Sales, Bull. Am. Phys. Soc. **33**, 721 (1988); W-H. Li, J. W. Lynn, H. A. Mook, B. C. Sales, and Z. Fisk, Phys. Rev. B **37**, 9844 (1988).

[17]J. W. Lynn, W-H. Li, H. A. Mook, B. C. Sales, and Z. Fisk, Phys. Rev. Lett. **60**, 2781 (1988).

[18]J. W. Lynn and W-H. Li, J. Appl. Phys. **64**, 6065 (1988).

[19]J. W. Lynn, W-H. Li, H. A. Mook, B. C. Sales, and Z. Fisk, J. Phys. (Paris) Colloq. **49**, C8-2153 (1988).

[20]A review of both theory and experiment that pertains to the oxide superconductors is given in *High Temperature Superconductivity,* edited by J. W. Lynn (Springer-Verlag, New York, 1990).

[21]R. J. Cava, B. Batlogg, C. H. Chen, E. A. Tietman, S. M. Zahurak, and D. Werder, Phys. Rev. B **36**, 5719 (1987).

[22]D. C. Johnston, S. K. Sinha, A. J. Jacobson, and J. M. Newsam, Physica **153-155C**, 572 (1988).

[23]B. Gillon, D. Petitgrand, A. Delapalme, P. Radhakrishna, and G. Collin, Physica **156-157B**, 851 (1989).

[24]J. W. Lynn, W-H. Li, S. Trevino, and Z. Fisk, Phys. Rev. B **40**, 5172 (1989).

[25]M. Sato, S. Shamoto, J. M. Tranquada, G. Shirane, and B. Keimer, Phys. Rev. Lett. **61**, 1317 (1988).

[26]G. Aeppli, S. M. Hayden, H. Mook, Z. Fisk, S-W. Cheong, D. Rytz, J. P. Remeika, G. P. Espinosa, and A. S. Cooper, Phys. Rev. Lett. **62**, 2052 (1989).

[27]K. B. Lyons, P. A. Fleury, L. F. Schneemeyer, and J. V. Waszczak, Phys. Rev. Lett. **60**, 732 (1988); K. B. Lyons and P. A. Fleury, J. Appl. Phys. **64**, 6075 (1988).

[28]F. Mezei, B. Farago, C. Pappas, Gy. Hutiray, L. Rosta, and L. Mihaly, Physica **153-155C**, 1669 (1988).

[29]G. Shirane, R. J. Birgeneau, Y. Endoh, P. Gehring, M. A. Kastner, K. Kitazawa, H. Kojima, I. Tanaka, T. R. Thurston, and K. Yamada, Phys. Rev. Lett. **63**, 330 (1989).

[30]See, for example, P. W. Anderson, Science **235**, 1196 (1987); P. W. Anderson, G. Baskaran, Z. Zou, and T. Hsu, Phys. Rev. Lett. **58**, 2790 (1987); V. J. Emery, *ibid.* **58**, 2794 (1987); R. H. Parmenter, *ibid.* **59**, 923 (1987); J. E. Hirsch, Phys. Rev. B **35**, 8726 (1987); Phys. Rev. Lett. **59**, 228 (1987); J. R. Schrieffer, X-G. Wen, and S-C. Zhang, *ibid.* **60**, 944 (1988).

[31]See, for example, R. J. Cava *et al.*, Phys. Rev. Lett. **58**, 1676 (1987).

[32]J. H. Brewer *et al.*, Phys. Rev. Lett. **60**, 1073 (1988).

[33]G. L. Squires, *Introduction to the Theory of Thermal Neutron Scattering* (Cambridge University Press, Cambridge, 1978).

[34]R. M. Moon, T. Riste, and W. C. Koehler, Phys. Rev. **181**, 920 (1969).

[35]The Nd moments order below 2 K. See K. N. Yang, J. M. Ferreira, B. W. Lee, M. B. Maple, W-H. Li, J. W. Lynn, and R. W. Erwin, Phys. Rev. B **40**, 10963 (1989); P. Fischer, B. Schmid, P. Bruesch, F. Stucki, and P. Unternahrer, Z. Phys. B **74**, 183 (1989).

[36]J. Akimitsu and Y. Ito, J. Phys. Soc. Jpn. **40**, 1621 (1976).

[37]See, for example, J. W. Lynn, P. Heller, and N. A. Lurie, Phys. Rev. B **16**, 5032 (1977).

[38]This domain average turns out to be the same regardless of the assumed spin direction in the tetragonal plane, assuming that the tetragonal symmetry is maintained and that initially the domains are equally populated.

[39]If the easy spin direction is actually the [110]-type direction, then this is not really a spin-flop transition, but rather a situation where the [110]-type domain grows at the expense of the $[1\bar{1}0]$-type domain.

[40]With the very strong similarities between our data and theirs, we are confident that if measurements to lower temperature were taken on that sample, that excellent agreement would be obtained with our results.

[41]P. Zolliker, D. E. Cox, J. M. Tranquada, and G. Shirane, Phys. Rev. B **38**, 6575 (1988).

[42]P. F. Miceli, J. M. Tarascon, L. H. Greene, P. Barboux, M. Giroud, D. A. Neumann, J. J. Rhyne, L. F. Schneemeyer, and J. V. Waszczak, Phys. Rev. B **38**, 9209 (1988).

[43]See, for example, K. Zhang, B. Dabrowski, C. U. Segre, D. G. Hinks, I. K. Schuller, J. D. Jorgensen, and M. Slaski, J. Phys. C **20**, L935 (1987).

[44]For a review, see R. Beyers and T. M. Shaw, Solid State Phys. **42**, 135 (1989). See also R. J. Cava, B. Batlogg, C. H. Chen, E. A. Tietman, S. M. Zahurak, and D. Werder, Phys. Rev. B **36**, 5719 (1987); N. C. Bartelt, T. L. Einstein, and L. T. Wille, Physica **161C** (1989); Phys. Rev. B **40**, 10759 (1989).

[45]At $x = \frac{1}{2}$, for example, in the ordered case we would have all the oxygen sites in one chain occupied, while in the adjacent chains on either side they would be unoccupied. We believe that it is unlikely that there would be significant correlations between chain layers along the c axis.

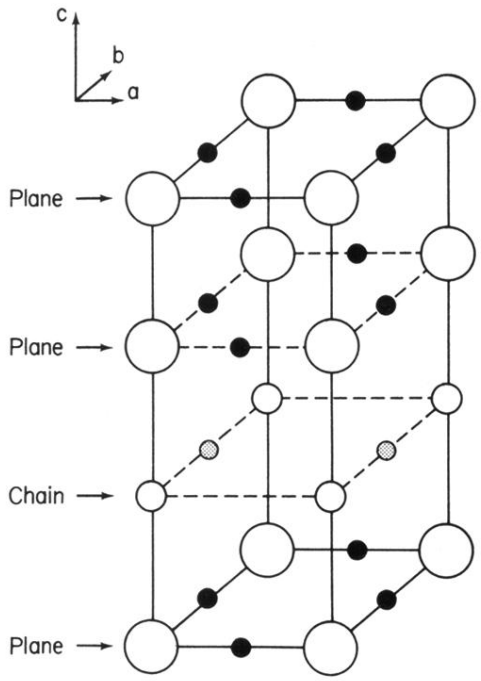

FIG. 1. The crystal structure of $\mathcal{R}Ba_2Cu_3O_7$, with only the Cu (open circles) and O ions (solid and shaded circles) in the copper-oxygen layers indicated for clarity. The rare-earth ion is located between the two plane layers, while the plane and the chain layers are separated by a BaO layer. The occupancy of the oxygen sites in the chain layer (shaded circles) can be readily varied from full occupancy ($x=1$) to full depletion ($x=0$).

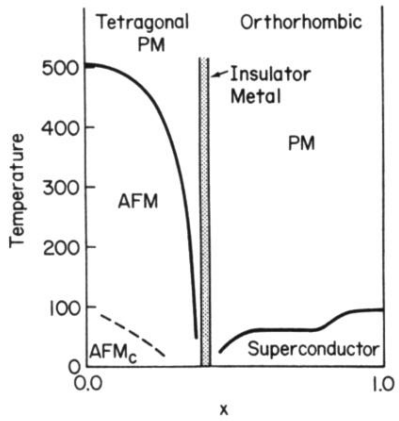

FIG. 2. Schematic phase diagram for $\mathcal{R}Ba_2Cu_3O_{6+x}$ as a function of oxygen concentration x on the chain sites. There are two antiferromagnetic phases in the small x regime: **AFM**, in which only the Cu spins in the plane layers are ordered, and $\mathbf{AFM}_C$, in which the Cu spins in the chain layers are also ordered. At large x or at very high temperatures the Cu ions are paramagnetic (**PM**).